

# Giant magnetoresistance in semiconductor / granular film heterostructures with cobalt nanoparticles

L.V. Lutsev<sup>1</sup>, A.I. Stognij<sup>2</sup>, and N.N. Novitskii<sup>2</sup>

<sup>1</sup>*A.F. Ioffe Physico-Technical Institute, Russian Academy of Sciences, 194021 St. Petersburg, Russia*

<sup>2</sup>*Scientific-Practical Materials Research Center of National Academy of Sciences of Belarus, 220072 Minsk, Belarus*

l\_lutsev@mail.ru

## Abstract

We have studied the electron transport in  $\text{SiO}_2(\text{Co})/\text{GaAs}$  and  $\text{SiO}_2(\text{Co})/\text{Si}$  heterostructures, where the  $\text{SiO}_2(\text{Co})$  structure is the granular  $\text{SiO}_2$  film with Co nanoparticles. In  $\text{SiO}_2(\text{Co})/\text{GaAs}$  heterostructures giant magnetoresistance effect is observed. The effect has positive values, is expressed, when electrons are injected from the granular film into the GaAs semiconductor, and has the temperature-peak type character. The temperature location of the effect depends on the Co concentration and can be shifted by the applied electrical field. For the  $\text{SiO}_2(\text{Co})/\text{GaAs}$  heterostructure with 71 at.% Co the magnetoresistance reaches 1000 ( $10^5$  %) at room temperature. On the contrary, for  $\text{SiO}_2(\text{Co})/\text{Si}$  heterostructures magnetoresistance values are very small (4%) and for  $\text{SiO}_2(\text{Co})$  films the magnetoresistance has an opposite value. High values of the magnetoresistance effect in  $\text{SiO}_2(\text{Co})/\text{GaAs}$  heterostructures have been explained by magnetic-field-controlled process of impact ionization in the vicinity of the spin-dependent potential barrier formed in the semiconductor near the interface. Kinetic energy of electrons, which pass through the barrier and trigger the avalanche process, is reduced by the applied magnetic field. This electron energy suppression postpones the onset of the impact ionization to higher electric fields and results in the giant magnetoresistance. The spin-dependent potential barrier is due to the exchange interaction between electrons in the accumulation electron layer in the semiconductor and  $d$ -electrons of Co. Existence of spin-polarized localized electron states in the accumulation layer results in the temperature-peak type character of the barrier and the magnetoresistance effect. Spin injector and spin-valve structure on the base of ferromagnet / semiconductor heterostructures with quantum wells with spin-polarized localized electrons in the semiconductor at the interface are considered.

## 1 Introduction

Electron spin transport in ferromagnet / semiconductor (FM / SC) heterostructures has recently become an active area of research. The manipulation of carrier spin in FM / SC heterostructures offers enhanced functionality of spin-electronic devices such as spin transistors, sensors and magnetic memory cells [1, 2]. FM / SC heterostructures are intended to employ as magnetoresistance cells and injectors of spin-polarized electrons in SCs [3, 4, 5]. For practical applications it is highly desirable to realize these effects at room temperature. Spin transport phenomena and magnetoresistance are observed on a number of heterostructures.

1. Spin injection into a non-magnetic SC is observed at low temperatures in magnetic SC / non-magnetic SC heterostructures [6, 7, 8] and in ferromagnetic metal / non-magnetic SC [9, 10, 11, 12, 13, 14]. At room temperature the spin injection reveals low efficiency.

2. Spin injection in the ferromagnetic metal / insulator / SC heterostructure is more efficient in comparison with the spin injection from ferromagnetic metal / SC heterostructures [15, 16, 17, 18, 19]. The maximum of the spin polarization of injected electrons is achieved for a MgO barrier on GaAs (47 % at 290 K) [17].
3. The giant magnetoresistance (GMR) is observed in metal magnetic multilayers [20, 21, 22, 23]. For three-layer structures, the typical values of GMR at room temperature lie in the range 5 - 8 %.
4. High values of tunneling magnetoresistance (TMR) are realized on the base of magnetic tunnel junction (MTJ) structures [24, 25, 26, 27, 28, 29, 30, 31, 32, 33, 34]. Spin-dependent tunneling is not only determined by the properties of ferromagnetic electrodes but also depends on the electronic structure of insulator barriers. The maximum TMR ratio of 500 % at room temperature was observed in the MTJ structure with the MgO barrier [34].
5. Extremely large magnetoresistance can be achieved by use magnetic-field-dependent avalanche breakdown phenomena [35, 36, 37, 38, 39, 40, 41, 42, 43]. Values of the magnetoresistance effect based on the avalanche breakdown reach  $10^5$  % in the Au / semi-insulating GaAs Schottky diode at room temperature [37].

Although important results in the spin injection and in the magnetoresistance have been obtained, the efficient spin injection at room temperature has not been achieved and for some applications it is necessary to use sensors with high magnetoresistance values. These problems can be resolved by using FM / SC heterostructures with spin-dependent potential barrier, which governs the kinetic energy of injected electrons and the onset of impact ionization [38, 39, 40]. In these heterostructures FM is a granular film with  $d$  (or  $f$ ) metal nanoparticles. In contrast with metal / SC structures with the Schottky barrier based on the magnetic-field-dependent avalanche breakdown phenomena [37, 41, 42, 43], the transparency of the spin-dependent potential barrier, which is formed in the spin-polarized accumulation electron layer in the SC near the interface, is characterized by the temperature-peak dependence and is different for different spin orientations of injected electrons. The barrier is due to the exchange interaction between  $d$  ( $f$ ) electrons in the FM at the interface and electrons in the SC, which polarizes electrons in the accumulation layer.

In this paper, we study the magnetoresistance in  $\text{SiO}_2(\text{Co})/\text{GaAs}$  and  $\text{SiO}_2(\text{Co})/\text{Si}$  heterostructures, where the  $\text{SiO}_2(\text{Co})$  is the granular  $\text{SiO}_2$  film with Co nanoparticles. Sample preparation and experimental results are presented in section 2. The effect is more expressed, when electrons are injected from the granular film into the SC, therefore, the magnetoresistance has been called the injection magnetoresistance (IMR) [38, 39]. For  $\text{SiO}_2(\text{Co})/\text{GaAs}$  heterostructures the IMR value reaches 1000 ( $10^5$  %) at room temperature, which is two-three orders higher than maximum values of the GMR in metal magnetic multilayers and the TMR in MTJ structures. On the contrary, for  $\text{SiO}_2(\text{Co})/\text{Si}$  heterostructures the magnetoresistance values are very small and for  $\text{SiO}_2(\text{Co})$  films the intrinsic magnetoresistance is of a negative value. The IMR effect has a temperature-peak type character and its location can be shifted by the applied electrical field. High values of the IMR effect in  $\text{SiO}_2(\text{Co})/\text{GaAs}$  heterostructures and the temperature-peak type character are explained in section 3 by the theoretical model of a magnetic-field-controlled avalanche process provided by electrons passed through the spin-dependent potential barrier in the accumulation layer at the interface [40]. In section 4 we consider FM / SC heterostructures with quantum wells with spin-polarized localized electrons in the SC at the interface as efficient room-temperature spin injectors and magnetic sensors. These heterostructures can be used as bioanalytical sensors with higher sensitivity in comparison with GMR-sensors [44, 45] and as injectors in spin-valve transistors and in spin field-effect

transistor (FET) structures [46, 47, 48].

## 2 Experimental results

### 2.1 Sample preparation

Experiments were performed on samples of amorphous silicon dioxide films containing cobalt nanoparticles grown (1) on gallium arsenide,  $(\text{SiO}_2)_{100-x}\text{Co}_x/\text{GaAs}$  (or shorter  $\text{SiO}_2(\text{Co})/\text{GaAs}$ ), (2) on silicon,  $(\text{SiO}_2)_{100-x}\text{Co}_x/\text{Si}$  (or shorter  $\text{SiO}_2(\text{Co})/\text{Si}$ ), and (3) on quartz substrates. n-GaAs substrates with thickness of 0.4 mm are of the (100)-orientation type. Electrical resistivity of GaAs chips was measured by the dc four-probe method at room temperature and was equal to  $0.93 \cdot 10^5 \Omega \cdot \text{cm}$ . The 0.4 mm n-Si substrates have the orientation of (100) and the resistivity of  $3.7 \Omega \cdot \text{cm}$ . Prior to the deposition process, substrates were polished by a low-energy oxygen ion beam [49, 50]. The roughness height of the polished surfaces did not exceed 0.5 nm.

The  $\text{SiO}_2(\text{Co})$  films were deposited by ion-beam co-sputtering of the composite cobalt-quartz target onto GaAs, Si and quartz substrates heated to  $200^\circ\text{C}$ . The concentration of Co nanoparticles in the silicon dioxide deposit was varied by changing the ratio of cobalt and quartz target areas. The film composition was determined by the nuclear physical methods of element analysis using a deuteron beam of the electrostatic accelerator (PNPI, Gatchina, Leningrad region, Russia). The cobalt to silicon atomic ratio was measured by the Rutherford backscattering spectrometry of deuterons. The oxygen concentration in films was determined by the method of nuclear reaction with deuterons at  $E_d = 0.9 \text{ MeV}$ :  $^{16}\text{O} + d \rightarrow p + ^{17}\text{O}$ . This technique is described in more detail elsewhere [51]. For the samples studied, the relative content of cobalt  $x$  and the film thickness are listed in Table 1. The average size of Co particles was determined by the small-angle X-ray scattering and increased as the concentration of  $x$  grows: from 2.7 nm at  $x = 38 \text{ at.}\%$  to 4.4 nm at  $x = 82 \text{ at.}\%$ . Cobalt particles are in the ferromagnetic state [52, 53, 54]. The samples with high concentration of Co (71 and 82 at.%) exhibit ferromagnetic behaviour confirmed by the presence of a domain structure (Figure 1) obtained with NT-MDT magnetic field microscope Solver HV-MFM. The period of the domain structure for the  $\text{SiO}_2(\text{Co})/\text{GaAs}$  sample with 82 at.% Co is equal to  $3.9 \mu\text{m}$ , which is smaller than the domain period for the same  $\text{SiO}_2(\text{Co})$  film on the Si substrate ( $6.0 \mu\text{m}$ ). The samples with low concentration of Co are superparamagnetic.

Electrical resistivity of  $\text{SiO}_2(\text{Co})$  films was measured by the dc four-probe method on  $\text{SiO}_2(\text{Co})/\text{quartz}$  heterostructures at room temperature. As the Co content increased, the resistivity of  $\text{SiO}_2(\text{Co})$  films decreased from  $1.46 \cdot 10^2 \Omega \cdot \text{cm}$  (38 at.%) to  $1.1 \Omega \cdot \text{cm}$  (82 at.%).

**Table 1.** Properties of  $\text{SiO}_2(\text{Co})$  films sputtered on GaAs, Si and quartz substrates.

Co concentration $x$ (at.%)	Film thickness (nm)		
	GaAs substrate	Si substrate	Quartz substrate
38	86	86	860
45	81	81	810
54	90	90	900
71	95	95	950
82	95	95	950

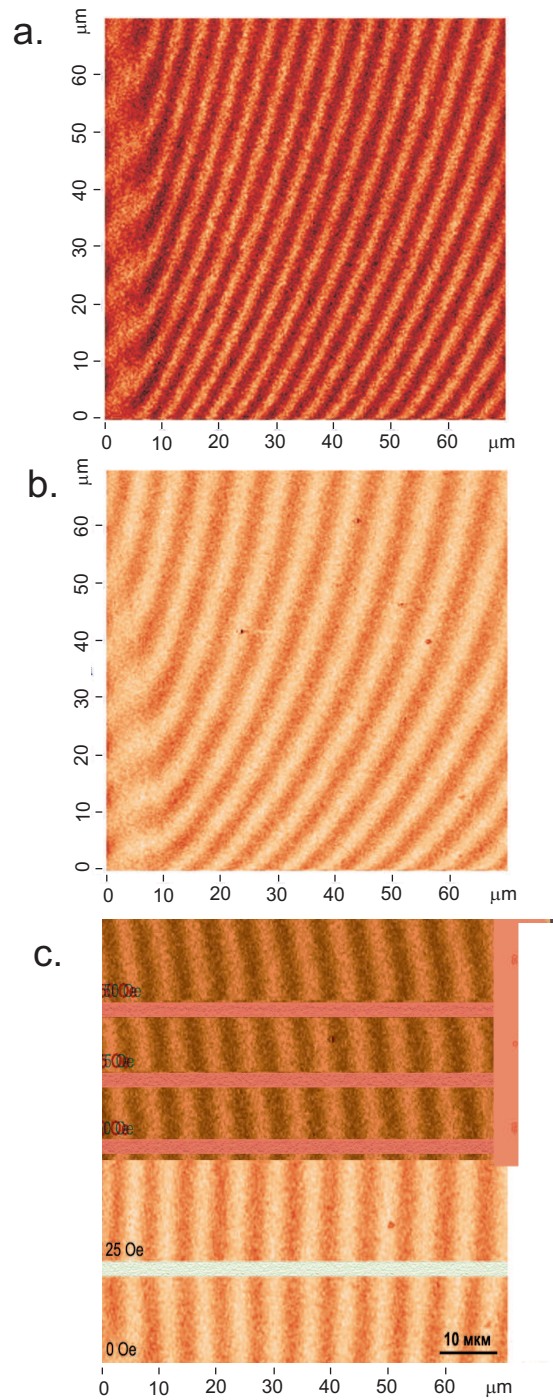


Figure 1: Magnetic field microscope image of the domain structure on samples with  $\text{SiO}_2(\text{Co})$  films with 82 at.% Co (a) on the GaAs substrate and (b) on the Si substrate. (c) Influence of the applied magnetic field on the domain structure on the  $\text{SiO}_2(\text{Co})/\text{Si}$  sample with 82 at.% Co.

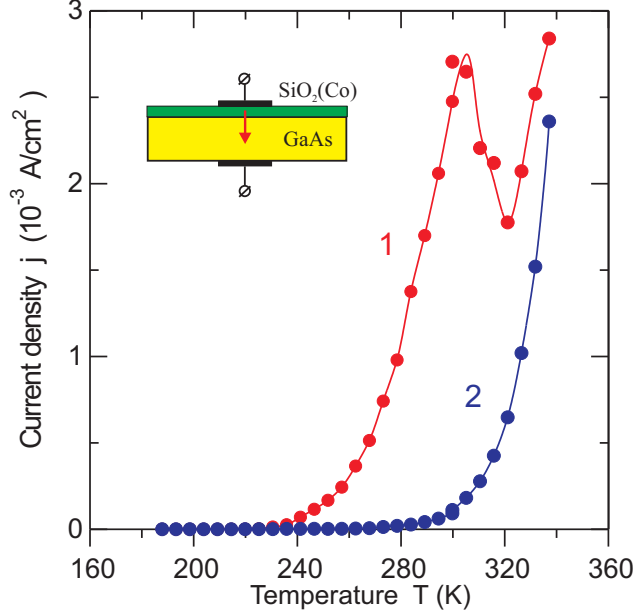


Figure 2: Temperature dependencies of the inject current  $j$  for the  $\text{SiO}_2(\text{Co})/\text{GaAs}$  structure with the Co concentration 71 at.% at the applied voltage  $U = 70$  V. (1) In the absence of a magnetic field, (2) in the magnetic field  $H = 10$  kOe.  $H$  is parallel to the surface of the  $\text{SiO}_2(\text{Co})$  film. Solid lines are guides for the eye.

## 2.2 Experiment

We have studied the electron transport and magnetoresistance in  $\text{SiO}_2(\text{Co})/\text{SC}$  heterostructures (Table 1). One contact was on the semiconductor substrate, and the other – on the  $\text{SiO}_2(\text{Co})$  granular film. All  $\text{SiO}_2(\text{Co})/\text{GaAs}$  samples and  $\text{SiO}_2(\text{Co})/\text{Si}$  samples with the Co concentration, which is equal to or lesser than 71 at.%, have current-voltage dependencies of the diode type. At positive voltages for structures of the diode type current-voltage characteristic electrons are injected from the granular film into the SC and the current density  $j$  is high. For the applied voltage  $U = 90$  V the current density reaches  $6.0 \cdot 10^{-2}$  A/cm<sup>2</sup>. In the case when the applied voltage  $U$  is negative, electrons drift from the SC into the granular film and the current density is low. For  $\text{SiO}_2(\text{Co})/\text{Si}$  heterostructure with high Co content (82 at.%), the current-voltage characteristic is close to the dependence of the Ohm type. Figure 2 shows temperature dependencies of the electron inject current density  $j$  for the  $\text{SiO}_2(\text{Co})/\text{GaAs}$  structure with the Co concentration  $x = 71$  at.% at the applied voltage  $U = 70$  V. The resistivity of GaAs is higher than the resistivity of the film and the applied voltage primarily falls on the SC substrate. We notice that at the temperature  $T = 320$  K in the absence of a magnetic field the inject current has local minimum. The electron inject current flowing from the granular film into the SC is suppressed by the magnetic field. The magnetic field  $H$  is equal to 10 kOe and is parallel to the surface plane of the granular film. At  $T > 320$  K temperature dependencies of the inject current in the absence of a magnetic field and in the field  $H$  are close.

Figure 3 illustrates the effect of the magnetic field on the current-voltage characteristic for the injection of electrons into the semiconductor for the  $\text{SiO}_2(\text{Co})/\text{GaAs}$  structure with

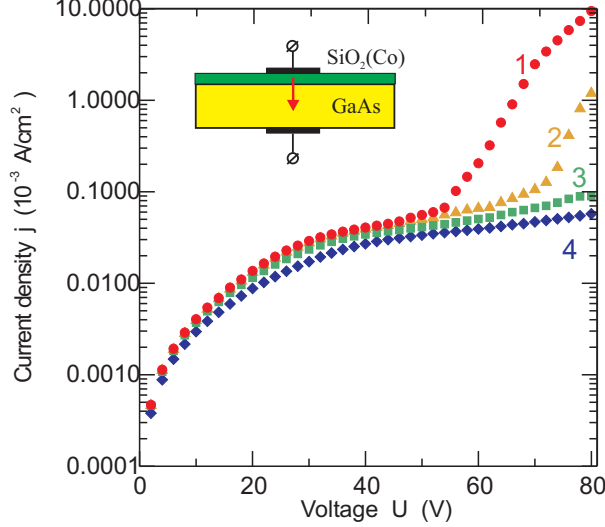


Figure 3: Current-voltage characteristic for the injection of electrons into the semiconductor for the  $\text{SiO}_2(\text{Co})/\text{GaAs}$  structure with 71 at.% Co at different magnetic fields: (1)  $H = 0$ , (2) 5 kOe, (3) 10 kOe, (4) 15 kOe.  $H$  is parallel to the surface of the  $\text{SiO}_2(\text{Co})$  film.

71 at.% Co. For  $U > 52$  V, a sharp increase in current due to the process of impact ionization is observed. The applied magnetic field postpones this process to higher electric fields. The magnetic field  $H$  is parallel to the film surface. If the magnetic field is perpendicular to the film surface, the dependence of the current on the magnetic field  $H$  is weaker because of the demagnetization factor of the film, but the magnetic suppression of the current is still observed.

By analogy with GMR and TMR coefficients [20, 21, 22, 23, 24, 25, 26, 27, 28, 29, 30, 31, 32, 33, 34], we define the injection magnetoresistance coefficient  $IMR$  as the ratio [38, 39, 40]

$$IMR = \frac{R(H) - R(0)}{R(0)} = \frac{j(0) - j(H)}{j(H)}, \quad (1)$$

where  $R(0)$  and  $R(H)$  are the resistances of the  $\text{SiO}_2(\text{Co})/\text{SC}$  heterostructure without a field and in the magnetic field  $H$ , respectively;  $j(0)$  and  $j(H)$  are the current densities flowing in the heterostructure in the absence of a magnetic field and in the field  $H$ . The IMR ratio for the  $\text{SiO}_2(\text{Co})/\text{GaAs}$  structure with 71 at.% Co at different applied voltages at room temperature (21°C) is shown in Figure 4 as a function of the magnetic field  $H$  parallel to the film. As seen from Figure 4, the IMR coefficient increases with the growth of the applied voltage. At the voltage  $U = 90$  V for this structure the value of IMR reaches up to 1000 ( $10^5$  %) at room temperature at the field  $H = 19$  kOe. This is two-three orders higher than maximum values of GMR in metal magnetic multilayers and TMR in MTJ structures.

The IMR ratio for  $\text{SiO}_2(\text{Co})/\text{GaAs}$  structures versus the Co concentration  $x$  in the in-plane field  $H = 20$  kOe at the applied voltage  $U = 60$  V for different current directions is presented in Figure 5. The IMR coefficient has maximum values for structures with Co concentrations in the range [54 - 71 at.%], when electrons are injected from the  $\text{SiO}_2(\text{Co})$  film into the SC. The IMR ratio decreases for structures with higher ( $x > 71$  at.%) and lower ( $x < 54$  at.%) Co concentrations. On the contrary, in the case of the opposite current direction (electrons drift from the SC into the granular film) the magnetoresistance effect becomes less expressed.

As we can see from Figures 4 and 5, for  $\text{SiO}_2(\text{Co})/\text{GaAs}$  structures the IMR coefficient

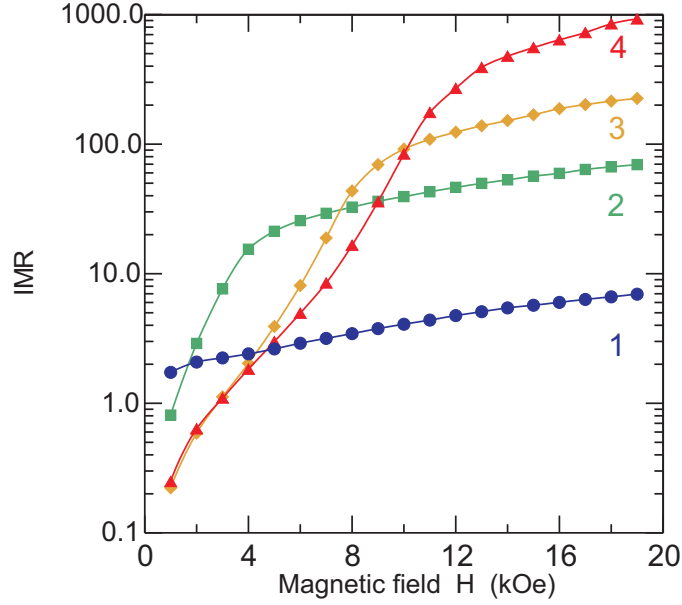


Figure 4: Injection magnetoresistance ratio, IMR, versus the magnetic field  $H$  at room temperature for the  $\text{SiO}_2(\text{Co})/\text{GaAs}$  structure with 71 at.% Co at applied voltages: (1)  $U = 60$  V, (2) 70 V, (3) 80 V, (4) 90 V.  $H$  is parallel to the surface of the  $\text{SiO}_2(\text{Co})$  film. Solid lines serve to guide the eye.

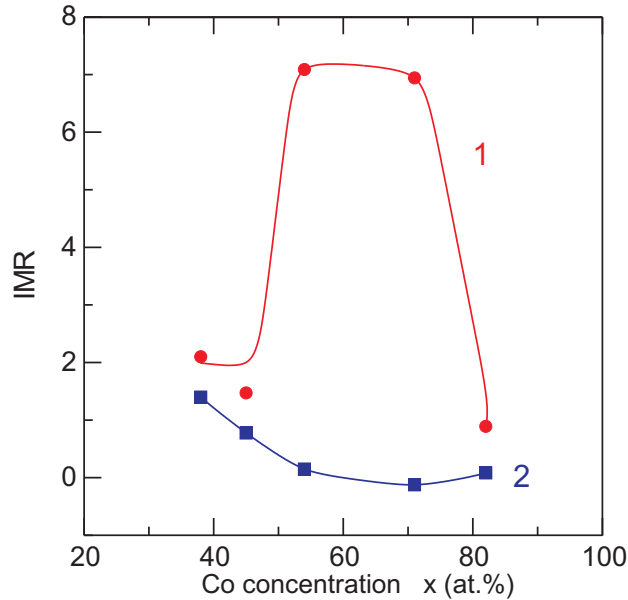


Figure 5: Magnetoresistance ratio, IMR, versus the Co concentration  $x$  for  $\text{SiO}_2(\text{Co})/\text{GaAs}$  structures in the field  $H = 20$  kOe at the applied voltage  $U = 60$  V for different current directions. (1) Electrons are injected from the  $\text{SiO}_2(\text{Co})$  film into GaAs, (2) electrons drift from GaAs into the granular film.  $H$  is parallel to the surface of the  $\text{SiO}_2(\text{Co})$  film. Solid lines serve to guide the eye.

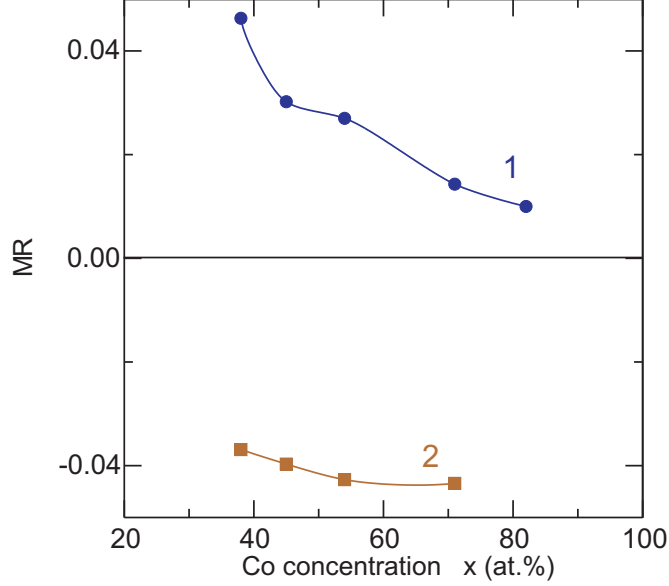


Figure 6: Magnetoresistance ratio, MR, versus the Co concentration  $x$  for (1)  $\text{SiO}_2(\text{Co})/\text{Si}$  structures and for (2)  $\text{SiO}_2(\text{Co})$  films in the in-plane magnetic field  $H = 20$  kOe. Solid lines serve to guide the eye.

can reach high values at room temperature. In contrast with this, for  $\text{SiO}_2(\text{Co})/\text{Si}$  structures magnetoresistance values are very small and the intrinsic magnetoresistance of  $\text{SiO}_2(\text{Co})$  films has negative values (Figure 6). The magnetoresistance ratio (MR) for  $\text{SiO}_2(\text{Co})$  films is determined by the relation analogous to Eq. (1). For  $\text{SiO}_2(\text{Co})/\text{Si}$  structures electrons are injected from the granular film into the Si substrate. Taking into account low values of the resistivity of Si substrates, experiments were carried out at the applied voltage  $U = 3$  V. For  $\text{SiO}_2(\text{Co})$  films the intrinsic magnetoresistance ratio was measured by the dc four-probe method on  $\text{SiO}_2(\text{Co})/\text{quartz}$  samples in the current-in-plane geometry at the applied voltage  $U = 60$  V at room temperature.

Temperature dependencies of the magnetoresistance can give useful information about the nature of the magnetoresistance effect. Figure 7 presents temperature dependencies of the intrinsic magnetoresistance for  $\text{SiO}_2(\text{Co})$  films with low ( $x = 38$  at.%) and high ( $x = 71$  at.%) Co concentrations and for the  $\text{SiO}_2(\text{Co}, 71 \text{ at.}\%)/\text{Si}$  structure. Experiments were carried out at the applied voltage  $U = 60$  V for  $\text{SiO}_2(\text{Co})$  films and at  $U = 3$  V for the  $\text{SiO}_2(\text{Co})/\text{Si}$  structure. The magnetic field  $H = 10$  kOe is parallel to the surface of the granular film. It can be seen that temperature decreasing causes to the growth of the absolute value of the intrinsic magnetoresistance for  $\text{SiO}_2(\text{Co})$  films. For the  $\text{SiO}_2(\text{Co})/\text{Si}$  structure electrons are injected from the granular film into the semiconductor and temperature decreasing leads to the change of the magnetoresistance sign.

Temperature dependencies of the IMR for  $\text{SiO}_2(\text{Co})/\text{GaAs}$  structures essentially differ from the above-mentioned dependencies for  $\text{SiO}_2(\text{Co})/\text{GaAs}$  structures and  $\text{SiO}_2(\text{Co})$  films. They have a peak type character (Figures 8 and 9). The temperature location of the peak depends on the Co concentration and can be shifted by the applied electrical field. Figure 8 shows temperature dependencies of the IMR for  $\text{SiO}_2(\text{Co})/\text{GaAs}$  with 71 at.% Co at different applied voltages, when electrons are injected from the granular film into the GaAs substrate. Increasing

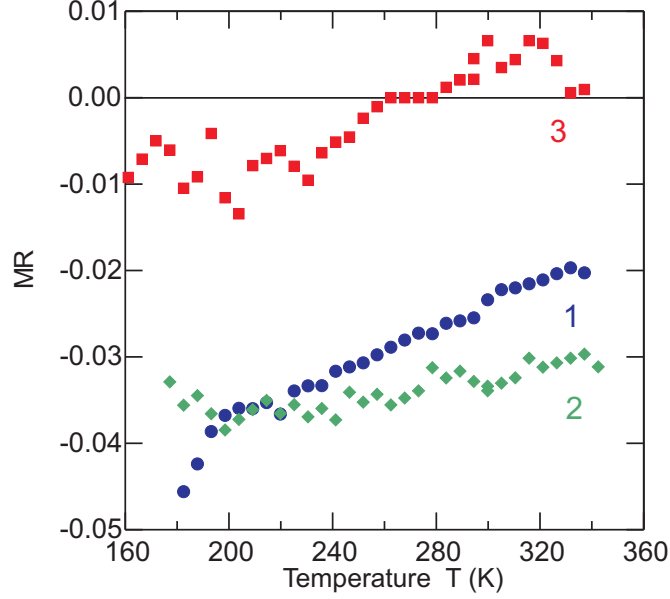


Figure 7: Temperature dependencies of the magnetoresistance, MR, for  $\text{SiO}_2(\text{Co})$  films (1) with  $x = 38$  at.% Co, (2) with  $x = 71$  at.% Co, and (3) for the  $\text{SiO}_2(\text{Co})/\text{Si}$  structure with  $x = 71$  at.% Co content in the in-plane magnetic field  $H = 10$  kOe.

voltage  $U$  causes to a shift of the peak to higher temperatures. At the same time, the voltage growth leads to an increase of the peak magnitude. For  $\text{SiO}_2(\text{Co})/\text{GaAs}$  structure with lower Co content ( $x = 38$  at.%, Figure 9), the temperature peak of the IMR has higher value of width. For the case, when electrons move from GaAs into the  $\text{SiO}_2(\text{Co})$  film, the IMR peak is located at higher temperature and its magnitude is lower.

### 3 Theoretical model and explanation of experimental results

#### 3.1 Theoretical model

Explanation of the IMR effect is based on the theoretical model of the magnetic-field-controlled avalanche process triggered by electrons passed through the spin-dependent potential barrier in the accumulation layer in the SC at the interface. The applied magnetic field reduces the transparency of the spin-dependent potential barrier. This leads to a decrease of the kinetic energy of injected electrons and to the suppression of the impact ionization onset.

Let us consider formation of the accumulation electron layer in the SC at the interface, the spin-dependent potential barrier and the IMR effect caused by the barrier [40]. In the FM/SC heterostructure the difference of chemical potentials  $\Delta\mu$  between the FM and the SC determines bending of the SC conduction band (Figure 10).  $d$ -electrons in the FM at the interface and electrons in the accumulation electron layer in the SC are coupled by the exchange interaction  $J_0(\vec{r} - \vec{R})$ . The Hamiltonian of the model is written in the form

$$\mathcal{H} = \mathcal{H}_e + \mathcal{H}_{ed} + \mathcal{H}_\varphi,$$

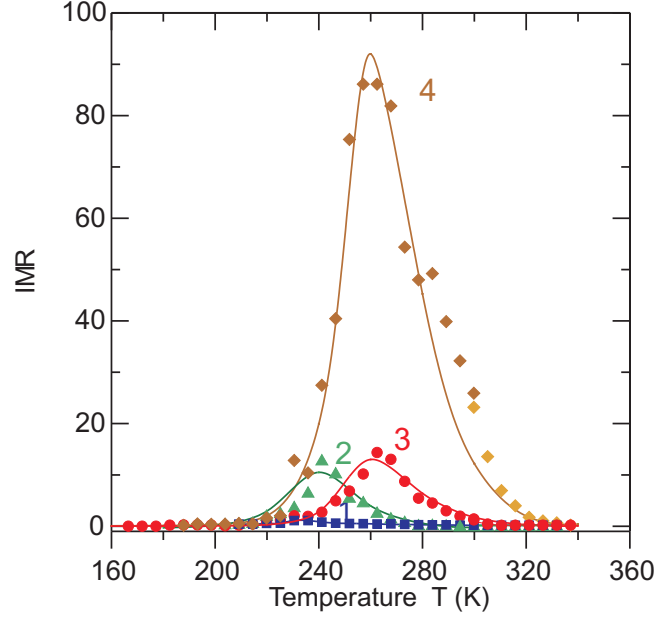


Figure 8: Temperature dependencies of the injection magnetoresistance, IMR, for the  $\text{SiO}_2(\text{Co})/\text{GaAs}$  structure with  $x = 71$  at.% Co content in the in-plane magnetic field  $H = 10$  kOe at applied voltages: (1)  $U = 40$  V, (2) 50 V, (3) 60 V, (4) 70 V. Solid lines are theoretical fittings.

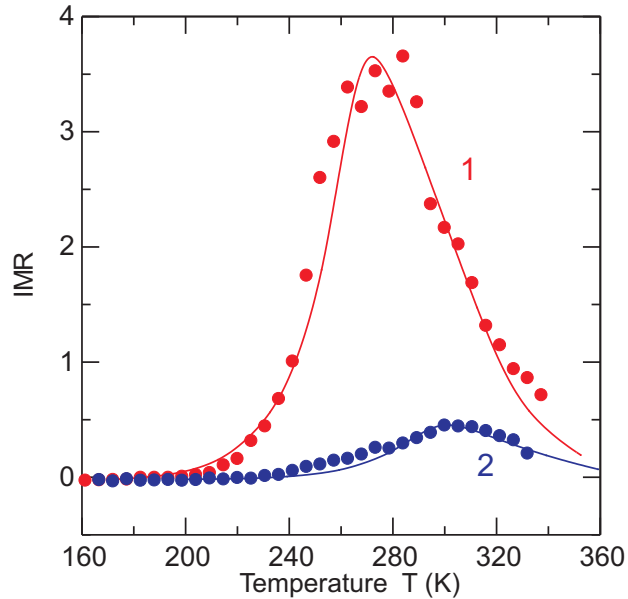


Figure 9: Temperature dependencies of the magnetoresistance, IMR, for the  $\text{SiO}_2(\text{Co})/\text{GaAs}$  structure with  $x = 38$  at.% Co content in the in-plane magnetic field  $H = 10$  kOe at the applied voltage  $U = 60$  V. (1) Electrons are injected from the  $\text{SiO}_2(\text{Co})$  film into GaAs, (2) electrons drift from GaAs into the granular film. Solid lines are theoretical fittings.

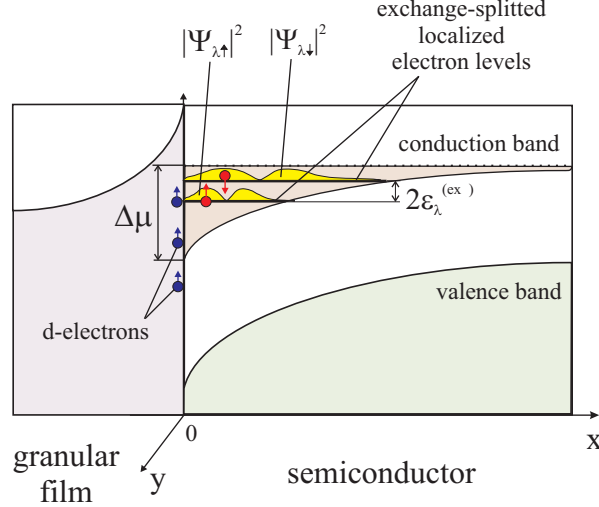


Figure 10: Electronic energy band structure at the contact region of the ferromagnet / semiconductor.

where

$$\mathcal{H}_e = \sum_{\alpha} \int \Psi_{\alpha}^{+}(\vec{r}) \left[ -\frac{\hbar^2}{2m} \Delta - \mu - e\varphi(\vec{r}) \right] \Psi_{\alpha}(\vec{r}) d\vec{r}$$

is the Hamiltonian of electrons with the mass  $m$  and the charge  $e$  in the SC in the electrical field with the potential  $\varphi(\vec{r})$ .  $\mu$  is the chemical potential.  $\Psi_{\alpha}^{+}(\vec{r}) = \sum_{\lambda} \psi_{\lambda}^{*}(\vec{r}) a_{\lambda\alpha}^{+}$ ,  $\Psi_{\alpha}(\vec{r}) = \sum_{\lambda} \psi_{\lambda}(\vec{r}) a_{\lambda\alpha}$  are the second-quantized wavefunctions of an electron with a spin  $\alpha = \uparrow, \downarrow$ .  $a_{\lambda\alpha}^{+}$ ,  $a_{\lambda\alpha}$  are the creation and annihilation Fermi operators, respectively, for an electron with the wavefunction  $\psi_{\lambda}(\vec{r})$  with the multiindex  $\lambda$ .

$$\mathcal{H}_{ed} = - \sum_{\vec{R}} \int J_0(\vec{r} - \vec{R}) (\vec{S}(\vec{R}), \vec{\sigma}(\vec{r})) d\vec{r}$$

is the exchange interaction Hamiltonian between the spin density  $\vec{\sigma}(\vec{r})$  of electrons in the SC and spins  $\vec{S}(\vec{R})$  of  $d$ -electrons in the FM. The vector spin density operator  $\vec{\sigma}(\vec{r})$  is determined by operators  $\Psi_{\alpha}(\vec{r})$ ,  $\Psi_{\alpha}^{+}(\vec{r})$

$$\sigma_x(\vec{r}) = \Psi_{\uparrow}^{+}(\vec{r}) \Psi_{\downarrow}(\vec{r}) + \Psi_{\downarrow}^{+}(\vec{r}) \Psi_{\uparrow}(\vec{r})$$

$$\sigma_y(\vec{r}) = -i\Psi_{\uparrow}^{+}(\vec{r}) \Psi_{\downarrow}(\vec{r}) + i\Psi_{\downarrow}^{+}(\vec{r}) \Psi_{\uparrow}(\vec{r})$$

$$\sigma_z(\vec{r}) = \Psi_{\uparrow}^{+}(\vec{r}) \Psi_{\uparrow}(\vec{r}) - \Psi_{\downarrow}^{+}(\vec{r}) \Psi_{\downarrow}(\vec{r}).$$

The Hamiltonian

$$\mathcal{H}_{\varphi} = -\frac{1}{8\pi} \int [\nabla\varphi(\vec{r})]^2 d\vec{r}$$

describes the classical inner electrostatic field  $\varphi(\vec{r})$ .

In order to find the effective exchange interaction between spins  $\vec{S}(\vec{R})$  of  $d$  electrons in the FM and the spin  $\vec{\sigma}^{(in)}(\vec{r})$  of an injected electron with the wavefunction  $\psi_{\alpha}^{(in)}(\vec{r})$  ( $\alpha = \uparrow, \downarrow$ ) and the spin-dependent potential barrier, the temperature diagram technique is used [55, 56]. Before this we consider formation of the accumulation electron layer.

### 3.1.1 Formation of the accumulation electron layer

In the self-consistent-field approximation of the diagram expansion electrons of the conduction band in the SC and the inner self-consistent electrical field are described by the following equations.

(1) Equation for the electron wavefunction in the SC

$$\left[ -\frac{\hbar^2}{2m} \frac{d^2}{dx^2} - e\varphi(x) \right] \chi_\nu(x) = \varepsilon_\nu^{(0)} \chi_\nu(x), \quad (2)$$

where  $\psi_\lambda(\vec{r}) = V^{-1/2} \chi_\nu(x) \exp(iq_y y + iq_z z)$  is the electron wavefunction in the volume  $V$  of the SC with the multiindex  $\lambda = (\nu, q_y, q_z)$  and the energy spectrum  $\varepsilon_\lambda = \varepsilon_\nu^{(0)} + \hbar^2(q_y^2 + q_z^2)/2m$ .

(2) The equation for the inner self-consistent electrical field

$$\Delta\varphi(\vec{r}) = 4\pi e \left\{ \sum_{\lambda, \omega_n} [G_{\lambda\uparrow\uparrow}(\vec{r}, \vec{r}, \omega_n) + G_{\lambda\downarrow\downarrow}(\vec{r}, \vec{r}, \omega_n) - G_{\lambda\uparrow\uparrow}^{(0)}(\vec{r}, \vec{r}, \omega_n) - G_{\lambda\downarrow\downarrow}^{(0)}(\vec{r}, \vec{r}, \omega_n)] \right\}, \quad (3)$$

where

$$G_{\lambda\alpha_1\alpha_2}(\vec{r}_1, \vec{r}_2, \omega_n) = \frac{\psi_\lambda^*(\vec{r}_1)\psi_\lambda(\vec{r}_2)\delta_{\alpha_1\alpha_2}}{\beta(i\hbar\omega_n - E_{\lambda\alpha_1} + \mu)}, \quad (4)$$

are electron Green functions (Figure 11(a)),  $\beta = 1/kT$ ,  $k$  is the Boltzmann constant,  $T$  is the temperature,  $\hbar\omega_n = (2n + 1)\pi/\beta$ ,  $n$  is an integer,

$$E_{\lambda\alpha} = \varepsilon_\lambda \mp \varepsilon_\lambda^{(\text{ex})}. \quad (5)$$

The upper sign in equation (5) corresponds to  $\alpha = \uparrow$ ; the lower sign, to  $\alpha = \downarrow$ . The energy  $\varepsilon_\lambda^{(\text{ex})}$  is determined by the exchange Hamiltonian  $\mathcal{H}_{ed}$  in the self-consistent-field approximation

$$\varepsilon_\lambda^{(\text{ex})} = - \sum_{\vec{R}} \int J_0(\vec{r} - \vec{R}) (\langle \vec{S}(\vec{R}) \rangle_0, \langle \vec{\sigma}(\vec{r}) \rangle_0) d\vec{r}. \quad (6)$$

$\langle \vec{S}(\vec{R}) \rangle_0$  and  $\langle \vec{\sigma}(\vec{r}) \rangle_0$  are the statistical-average  $d$ -electron spin in the FM and the electron spin density in the SC, respectively.  $G_{\lambda\alpha\alpha}^{(0)}$  are electron Green functions determined in the single SC in the absence of the electrical field.

(3) The relationship between the chemical potential  $\mu$  and the electron concentration  $n_0$  in the single SC

$$n_0 = \frac{8\pi e}{V} \sum_{\vec{q}=(q_x, q_y, q_z)} n_F[\beta(\hbar^2|\vec{q}|^2/2m - \mu)]. \quad (7)$$

where  $n_F(a) = [\exp(a) + 1]^{-1}$ .

Equations (2), (3), (7) are simultaneous equations in unknowns: the wave function  $\chi_\nu(x)$ , the energy  $\varepsilon_\nu^{(0)}$ , the electrical potential  $\varphi(x)$ , and the chemical potential  $\mu$  in the SC. Taking into account that at the interface of the heterostructure ( $x = 0$ ) the potential  $\varphi(x)$  is determined by the difference of chemical potentials  $\Delta\mu$  between the SC and the FM,  $\varphi(0) = \Delta\mu/e$ , and at a great distance from the interface, when  $x \rightarrow \infty$ , the potential  $\varphi(x)$  tends to zero, we numerically can solve equations (2), (3), (7).

a.

$$G_{\lambda\uparrow\uparrow}(\mathbf{r}_1, \mathbf{r}_2, \omega_n) = \begin{array}{c} \text{---} \triangleright \text{---} \\ r_1 \qquad r_2 \end{array}$$

$$G_{\lambda\downarrow\downarrow}(\mathbf{r}_1, \mathbf{r}_2, \omega_n) = \begin{array}{c} \text{---} \blacktriangleright \text{---} \\ r_1 \qquad r_2 \end{array}$$

b.

$$\beta J_0(\mathbf{r}-\mathbf{R}) = \begin{array}{c} \text{---} \text{~~~~~} \text{---} \\ r \qquad \qquad \qquad R \end{array}$$

$$\beta J^{(\text{eff})}(\mathbf{r}, \mathbf{R}, \omega_n) = \text{---} + \begin{array}{c} \text{---} \text{---} \\ \text{---} \text{---} \end{array} + \begin{array}{c} \text{---} \text{---} \\ \text{---} \text{---} \end{array}$$

Figure 11: (a) Temperature electron Green functions with the spin  $\uparrow$  and  $\downarrow$ . (b) Bare and effective exchange interactions.

### 3.1.2 The effective exchange interaction and the spin-dependent potential barrier

The effective exchange interaction and the spin-dependent potential barrier for injected electrons are found in the next approximation of the diagram expansion. This is the one-loop approximation with respect to the bare exchange interaction  $J_0(\vec{r} - \vec{R})$  (figure 11(b)). In this approximation we take into account solutions of equations (2), (3), (7) made in the self-consistent-field approximation and find the effective exchange interaction

$$J^{(\text{eff})}(\vec{r}, \vec{R}, \omega_n) = J_0(\vec{r} - \vec{R}) + J_1(\vec{r}, \vec{R}, \omega_n),$$

where the interaction  $J_1$  has the form

$$J_1(\vec{r}, \vec{R}, \omega_n) = -\beta \int \int J_0(\vec{r} - \vec{r}_1) \sum_{k, \lambda_1, \lambda_2} [G_{\lambda_1\uparrow\uparrow}(\vec{r}_1, \vec{r}_2, \omega_k) G_{\lambda_2\uparrow\uparrow}(\vec{r}_1, \vec{r}_2, \omega_k + \omega_n) + G_{\lambda_1\downarrow\downarrow}(\vec{r}_1, \vec{r}_2, \omega_k) G_{\lambda_2\downarrow\downarrow}(\vec{r}_1, \vec{r}_2, \omega_k + \omega_n)] J_0(\vec{r}_2 - \vec{R}) d\vec{r}_1 d\vec{r}_2. \quad (8)$$

In the relation (8) the Green functions  $G_{\lambda\alpha_1\alpha_2}$  (4) are expressed via wavefunctions  $\psi_\lambda(\vec{r})$ , the chemical potential  $\mu$  and the electron energy  $E_{\lambda\alpha}$  (5). The interaction  $J_1$  is of the RKKY-type (Ruderman, Kittel, Kasuya, Yosida [57, 58, 59]). Spins of electrons in the accumulation layer shield spins of  $d$ -electrons in the FM at the interface. As the result of this shielding, the short-range exchange interaction  $J_0(\vec{r} - \vec{R})$  is transformed into the long-range effective exchange interaction  $J^{(\text{eff})}(\vec{r}, \vec{R}, \omega_n)$ , which changes its sign at a some distance from the interface (figure 12). To find the numerical solution, we assume that  $J_0(\vec{r} - \vec{R}) = J_0 \exp(-\xi|\vec{r} - \vec{R}|)$  in equations (6), (8), where  $\xi$  is the reciprocal radius of the exchange interaction and  $J_0$  is determined by the Coulomb interaction with  $d$ -electrons on a FM atom [60]. Calculations have been drawn, when  $\omega_n = 0$ ,  $\vec{R} = 0$ ,  $\xi = 10 \text{ nm}^{-1}$ ,  $J_0 = 2 \text{ eV}$ ,  $|\langle \vec{S}(\vec{R}) \rangle_0| = 1/2$ ,  $|\langle \vec{\sigma}(\vec{r}) \rangle_0| = 1/2|\psi_\lambda(\vec{r})|^2$ ,  $\Delta\mu = 150 \text{ meV}$ ,  $n_0 = 1 \times 10^{15} \text{ cm}^{-3}$  at  $T = 300 \text{ K}$  for the cubical crystal FM lattice with the lattice constant  $a = 0.23 \text{ nm}$ . At the distance  $r_0$  the exchange interaction  $J_1$  has a maximum opposite value. If the accumulation layer (quantum well) contains a great number of electron states, the distance  $r_0$  can be evaluated as the half of the period of the Ruderman-Kittel function,  $r_0 \approx \frac{1}{2}(\pi/3n_s)^{1/3}$  [57, 58, 59], where  $n_s$  is the electron density at the interface.

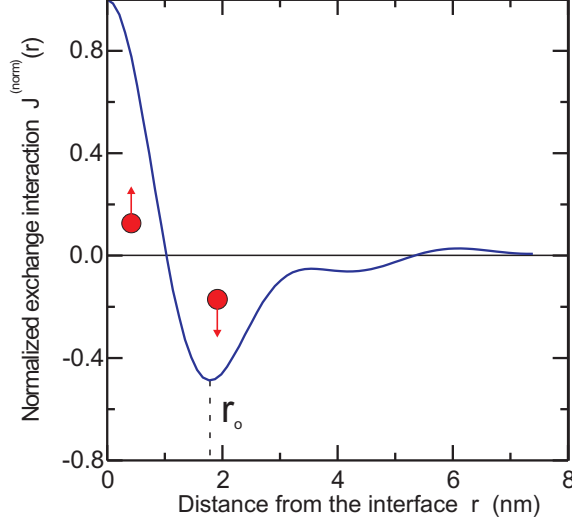


Figure 12: Normalized exchange interaction  $J^{(\text{norm})}(r) = J_1(\vec{r}, 0, 0)/J_1(0, 0, 0)$  for the heterostructure with the difference of chemical potentials  $\Delta\mu = 150$  meV and with the electron concentration  $n_0 = 1 \times 10^{15} \text{ cm}^{-3}$  in the SC at  $T = 300$  K.

In order to find the spin-dependent potential barrier, we assume that the magnetic field  $\vec{H}$  is parallel to the axis Oz. Then, the height of the energy barrier formed by the effective exchange interaction for injected spin-polarized electrons, which move from the interface, is determined by the relation

$$W = \sum_{\vec{R}} \int \langle \sigma_z^{(in)}(\vec{r}) \rangle J^{(\text{eff})}(\vec{r}, \vec{R}, 0) \langle S_z(\vec{R}) \rangle_0 d\vec{r}, \quad (9)$$

where  $\langle \sigma_z^{(in)}(\vec{r}) \rangle = \langle \psi_{\uparrow}^{(in)*}(\vec{r}) \psi_{\uparrow}^{(in)}(\vec{r}) - \psi_{\downarrow}^{(in)*}(\vec{r}) \psi_{\downarrow}^{(in)}(\vec{r}) \rangle$ ,  $\langle S_z(\vec{R}) \rangle_0$  is the  $z$ -projection of the statistical-average  $d$ -electron spin at the site  $\vec{R}$  at the interface. For calculation of  $W$  we assume that the spin density  $\langle \sigma_z^{(in)}(\vec{r}) \rangle = 1/2 \cdot \delta(r - r_0)$ . We have found, that, if the accumulation layer contains a small number of localized electron states  $\chi_{\nu}(x)$ , which are determined by equation (2), then these states give the main contribution to the exchange interaction  $J_1$  in equation (8) and to the height of the energy barrier  $W$  (9). The maximum of the barrier is observed, when the accumulation layer has two sublevels of an exchange-split localized electron state (Figure 10). Exchange-split localized states have high values of the exchange energy  $\varepsilon_{\lambda}^{(\text{ex})}$  (6) and this causes to high values of the barrier  $W$  (9). If the accumulation layer does not contain localized states, the magnitude of  $W$  sharply falls. Dependencies of  $W$  on the difference of chemical potentials  $\Delta\mu$  and temperature dependencies are presented in [40].

### 3.1.3 The IMR effect

The observed IMR effect can be explained by the developed theoretical model. Applied electrical field bends the SC conduction band (Figure 13). Two ways of the spin-polarized current injected into the SC can be supposed: (1) injected electrons surmount the spin-dependent potential barrier  $W$  at the distance  $r_0$  from the interface, (2) spin-polarized electrons tunnel from sublevels of the exchange-split localized states. Let us consider the first way. In the absence of an external magnetic field, the domain structure of the granular film (Figure 1)

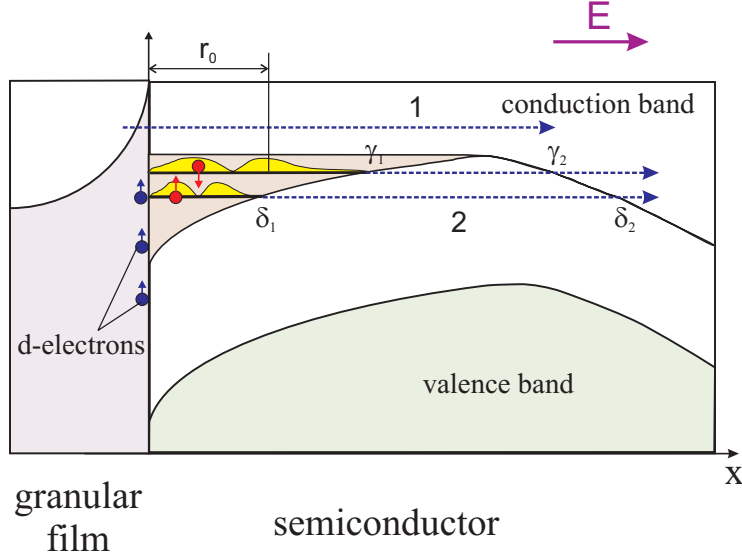


Figure 13: Schematic band diagram at the applied electrical field at the contact region of the ferromagnet / semiconductor. (1) Surmounting injected electrons over the spin-dependent potential barrier formed by localized states at the distance  $r_0$  from the interface, (2) tunneling from exchange-split localized states.

induces corresponding spin orientations of electrons localized in the accumulation layer and this domain structure has domain walls (Figure 14). In this case, electrons injected from the granular film can cross through the accumulation layer without a loss of their spin polarization and without surmounting the potential barrier on channels close to domain walls (trajectories with points  $a$ ). In the magnetic field of high values, when domains disappear, spin polarized electrons moving in the SC from the interface must surmount the potential barrier at the distance  $r_0$  (trajectories with points  $b$ ). Electrons surmounted the potential barrier trigger the process of impact ionization. According to [61], the voltage drop is concentrated mainly in the vicinity of the barrier. Consequently, the avalanche process originates in this vicinity region. The current density  $j$  flowing in the heterostructure is determined by the concentration of injected electrons  $n$ , the average velocity  $v$  and the multiplication factor  $M$  of the avalanche process,  $j = Menv$ . We suppose that in the absence of a magnetic field electrons cross through the points  $a$  and in the magnetic field electrons surmount the barrier through the points  $b$ . Then, taking into account that  $n_a = n_{int} \exp(eU_a/kT)$ ,  $n_b = n_{int} \exp[(eU_b - W)/kT]$ , where  $n_{int}$  is the electron concentration at the interface at the Fermi level,  $U_a$  and  $U_b$  are differences of potentials between the interface and points  $a$  and  $b$ , respectively, from equation (1) for the tunnel opaque potential barrier we get

$$IMR(W, T) = \frac{M_a n_a v_a}{M_b n_b v_b} - 1 = A \exp\left(\frac{W}{kT}\right) - 1. \quad (10)$$

The coefficient  $A$  is equal to  $M_a v_a / M_b v_b \exp[e(U_a - U_b)/kT]$ . It is need to notice that the relation (10) is truthful for high values of the magnetic field, when domains disappear. Taking into account that the energy barrier  $W$  sharply depends on temperature [40], in the first approximation the temperature dependence of the IMR is determined by the term  $\exp(W/kT)$ .

In the second case of the injected spin-polarized current, electrons with the spin  $\alpha$  and the

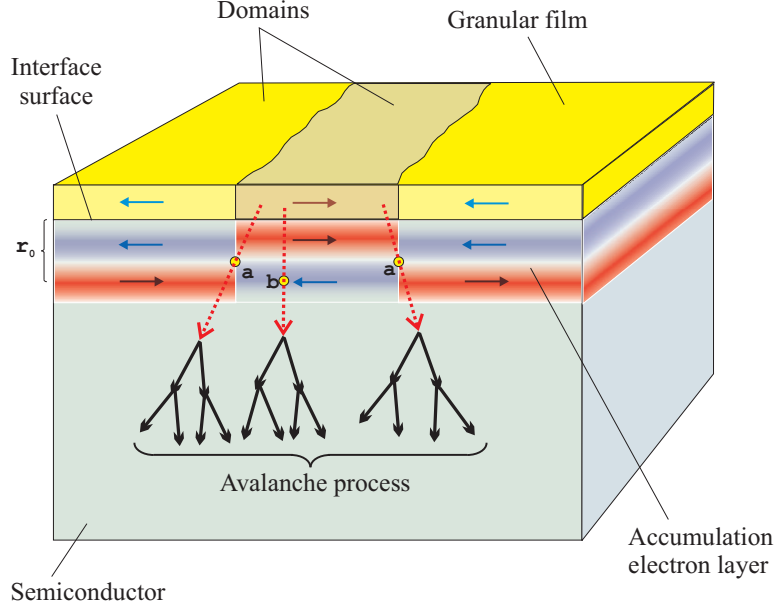


Figure 14: Trajectories without spin-flip scattering of injected electrons and without surmounting the potential barrier on the accumulation layer (points *a*) and trajectories with surmounting the potential barrier (points *b*).

energy  $E_{\lambda\alpha}$  (5) tunnel from sublevels of the exchange-split localized states. In the absence of an external magnetic field because of the existence of the domain structure in the granular film, spin orientations of localized electrons on sublevels in the accumulation layer are different for neighbouring regions corresponding to domains. In this case, tunneling occurs on channels close to domain walls. In the magnetic field of high values, domains disappear and the tunneling transparency decreases. The coefficient of the tunneling transparency from the state  $E_{\lambda\alpha}$  is [62]

$$D_{\lambda\alpha} = \exp \left\{ -\frac{2}{\hbar} \int_{\gamma_1(\delta_1)}^{\gamma_2(\delta_2)} | [2m(\bar{V}(x) - E_{\lambda\alpha}) ]^{1/2} | dx \right\},$$

where  $\bar{V}(x)$  is the potential energy of the barrier.

It is need to notice that the magnetic field can act on the avalanche process directly. The application of a magnetic field increases the density of states at the bottom of the lowest Landau level, causing electrons to occupy states with lower energy [37]. Electrons orbitals become more localized in the vicinity of donor ions and the overlap by their tails is reduced. Accordingly, the current decreases since fewer electrons can take part in the impact ionization process. The second mechanism of the magnetic-field action is quasi-neutrality breaking of the space-charge effect, where insufficient charge is present to compensate electrons injected into the SC [63]. The above-mentioned factors do not explain the observed temperature-peak type dependence of the IMR effect, but they can enhance the IMR value.

### 3.2 Explanation of the experiment

In order to explain high values of the IMR effect in  $\text{SiO}_2(\text{Co})/\text{GaAs}$  heterostructures and the temperature-peak type character, we use the developed theoretical model. The developed

theory can be applied for these heterostructures, if the size of Co nanoparticles is less than the thickness  $l$  of the accumulation layer. In this case, the granular film can be considered as continuous and can be characterized by statistical-average parameters. The thickness  $l$  depends on the difference of the chemical potentials  $\Delta\mu = \mu_g - \mu_s$ , where  $\mu_s$  is the chemical potential in the SC and  $\mu_g$  is the chemical potential in the granular film. In the first approximation, the chemical potential  $\mu_g$  is given by

$$\mu_g = \mu_{\text{SiO}_2}(x_{\text{SiO}_2}/100) + \mu_{\text{Co}}(x_{\text{Co}}/100), \quad (11)$$

where  $\mu_{\text{SiO}_2}$ ,  $\mu_{\text{Co}}$  are the chemical potentials of the  $\text{SiO}_2$  matrix and Co nanoparticles;  $x_{\text{SiO}_2}$ ,  $x_{\text{Co}}$  are the atomic concentrations of the  $\text{SiO}_2$  and Co in percents, respectively. The difference  $\Delta\mu$  between chemical potentials of the GaAs and the  $\text{SiO}_2(\text{Co})$  granular film and between chemical potentials of the Si substrate and the granular film can be estimated from well known values of the energy of the thermoelectron emission. For the given materials the differences of the chemical potentials are  $\mu_{\text{SiO}_2} - \mu_{\text{Co}} = 0.59$  eV,  $\mu_{\text{SiO}_2} - \mu_{\text{GaAs}} = 0.62$  eV,  $\mu_{\text{Co}} - \mu_{\text{GaAs}} = 0.03$  eV,  $\mu_{\text{SiO}_2} - \mu_{\text{Si}} = 0.95$  eV,  $\mu_{\text{Co}} - \mu_{\text{Si}} = 0.36$  eV [64].

In order to solve equations (2), (3), (7) in the approximation of the continuous granular film model, we need to find the surface probability of the Co particle distribution at the interface. We assume that at the interface Co particles are randomly allocated with the surface probability

$$s = p^{2/3} = \left[ \frac{x_{\text{Co}}v_{\text{Co}}}{x_{\text{Co}}v_{\text{Co}} + (100 - x_{\text{Co}})v_{\text{SiO}_2}} \right]^{2/3},$$

where  $p$  is the relative Co volume,  $v_{\text{Co}} = m_{\text{Co}}/\varrho_{\text{Co}}N_A$ ,  $v_{\text{SiO}_2} = m_{\text{SiO}_2}/\varrho_{\text{SiO}_2}N_A$  are atomic and molecular volumes for the Co and the  $\text{SiO}_2$  matrix;  $m_{\text{Co}}$ ,  $m_{\text{SiO}_2}$  are the respective atomic and molecular masses;  $\varrho_{\text{Co}}$ ,  $\varrho_{\text{SiO}_2}$  are the densities of Co particles and the  $\text{SiO}_2$  matrix;  $N_A$  is the Avogadro number. For calculations we use  $m_{\text{Co}} = 58.93$  a.m.,  $m_{\text{SiO}_2} = 60.09$  a.m.,  $\varrho_{\text{Co}} = 8.90$  g/cm<sup>3</sup>,  $\varrho_{\text{SiO}_2} = 2.26$  g/cm<sup>3</sup> [65]. According to the continuous granular film approximation, we must made substitutions  $\langle \vec{S}(\vec{R}) \rangle_0 \rightarrow s \langle \vec{S}(\vec{R}) \rangle_0$  and  $\langle S_z(\vec{R}) \rangle_0 \rightarrow s \langle S_z(\vec{R}) \rangle_0$  in relations (6) and (9), respectively.

Using the developed model, we have found the electron wavefunction  $\chi_\nu(x)$  (2), the inner self-consistent electrical field  $\varphi(\vec{r})$  (3), and the energy barrier  $W$  (9). Calculations have been made for the effective exchange interaction  $J_0(\vec{r} - \vec{R}) = J_0 \exp(-\xi|\vec{r} - \vec{R}|)$  with  $J_0 = 2$  eV,  $\xi = 2$  nm<sup>-1</sup> [60]. For  $\text{SiO}_2(\text{Co})/\text{GaAs}$  heterostructures at the given temperatures 160 - 340°C the thickness  $l$  of the accumulation layer is in the range 8 - 50 nm. The size of Co nanoparticles is less than the thickness  $l$ , and the approximation of the continuous granular film is truthful. Heterostructures possess localized electron states in the accumulation layer at the interface. In contrast, for  $\text{SiO}_2(\text{Co})/\text{Si}$  heterostructures due to higher values of the difference of the chemical potentials  $\Delta\mu$  at the interface the potential depth of the accumulation layer is deeper. This leads to higher electron concentration at the interface and to more efficient shielding of Co spins. As a result of this, the accumulation layer has small thickness without any localized states. The absence of localized states in  $\text{SiO}_2(\text{Co})/\text{Si}$  heterostructures explains small values of the barrier  $W$  (9) and small values of the IMR effect (figures 6, 7) in comparison with IMR values in  $\text{SiO}_2(\text{Co})/\text{GaAs}$  heterostructures (figures 4, 5, 8, 9). Let us consider IMR dependencies on the Co concentration, temperature and the magnetic field.

### 3.2.1 IMR dependence on the Co concentration

The dependence of the IMR on the Co concentration  $x$  for  $\text{SiO}_2(\text{Co})/\text{GaAs}$  structures, when electrons are injected from the  $\text{SiO}_2(\text{Co})$  film (figure 5), demonstrates high IMR values for the concentration range  $x = 54 - 71$  at.% and low IMR values for lower and higher Co concentrations. From the developed model it is found that structures with  $x = 54 - 71$  at.% have one - two electron localized states with high energies  $\varepsilon_\lambda^{(\text{ex})}$  (6), which leads to high barrier  $W$  at room temperature. Heterostructures with lower Co concentration possess greater number of localized states in the accumulation layer with energies  $\varepsilon_\lambda^{(\text{ex})}$  of small values. For these structures the IMR coefficient is low. If the Co concentration  $x > 71$  at.%, the accumulation layer has small thickness without localized states and is transparent for current.

### 3.2.2 Temperature dependencies of the IMR

At the interface the electron concentration increases with temperature increasing. At low temperatures the accumulation layer contains large number of exchange-splitting localized states with small energies  $\varepsilon_\lambda^{(\text{ex})}$ . Temperature increasing induces thinning of the accumulation layer, a decrease of the localized state number, an increase of energies  $\varepsilon_\lambda^{(\text{ex})}$ , and a growth of the barrier  $W$ . At a certain temperature the accumulation layer contains one exchange-splitting level and the magnitude of  $W$  reaches the maximum value. The further temperature growth gives higher electron concentration at the interface, more efficient shielding of Co spins, and thinner thickness of the accumulation layer. When the sublevel, on which electrons have spin orientations opposite to Co spins, crosses the Fermi level, the height of the potential barrier  $W$  sharply decreases. In Figure 2 for the  $\text{SiO}_2(\text{Co})/\text{GaAs}$  structure with the Co content 71 at.% crossing of the Fermi level is manifested as a fall on the temperature dependence of the inject current at  $T = 320$  K at the applied voltage  $U = 70$  V. This fall in the current corresponds to the disappearance of the IMR effect at 320 K,  $U = 70$  V in Figure 8.

The temperature-peak type character of the IMR effect is presented in figures 8, 9. Maxima of peaks correspond to one exchange-splitting level in the accumulation layer. Neglecting spin-polarized tunneling from exchange-splitting localized states, we fit experimental results using the relation (10). The barrier  $W$  is given by equation (9) and the amplitude  $A$  in the relation (10) is determined to reach the best fit of the peak height. According to the developed model, the peak width is inversely proportional to the magnitude of the surface probability  $s$  of the Co particle distribution at the interface. Decreasing the Co content results in the decrease of the surface probability  $s$ : from  $s = 0.52$  ( $x = 71$  at.% Co) to  $s = 0.26$  ( $x = 38$  at.% Co). This corresponds to the observed increase of the peak width with Co concentration decreasing: from  $\Delta T = 37$  K ( $x = 71$  at.% Co) to  $\Delta T = 62$  K ( $x = 38$  at.% Co).

Locations of IMR temperature peaks can be shifted by the applied electrical field. These shifts can be explained by the change of the electron concentration at the interface under the electrical field action. The applied field causes to an electron depletion in the SC at the interface. As a result of this, at high field magnitudes it is need higher temperatures to form the accumulation layer with one exchange-splitting level. In order to take into account the action of the electrical field for the  $\text{SiO}_2(\text{Co})/\text{GaAs}$  structure with the Co content 71 at.% in Figure 8, we use the following differences of the chemical potentials  $\Delta\mu$ : 0.201 eV ( $U = 40$  V), 0.197 eV ( $U = 50$  V), 0.187 eV ( $U = 60$  V and 70 V).

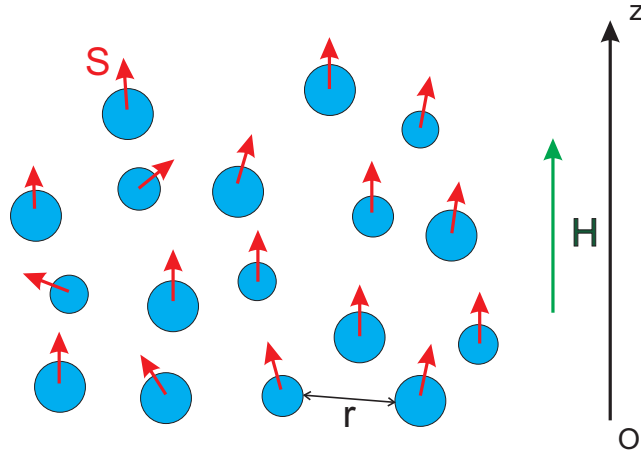


Figure 15: Alignment of spins of Co particles at the interface along the magnetic field direction. Distance  $r$  between Co particles is a random parameter.

### 3.2.3 IMR dependencies on the magnetic field

At last, we consider IMR dependencies on the magnetic field for  $\text{SiO}_2(\text{Co})/\text{GaAs}$  structures. As we can see from Figure 4, at magnetic fields of low values the IMR grows greater than at high magnetic fields. The high growth of the IMR can be explained by changes of the domain structure, which disappears at  $H \approx 3 - 4$  kOe. Slow IMR increasing at magnetic fields of high values can be due to alignment of different spin orientations of randomly allocated Co particles at the interface (Figure 15). Magnetic field polarizes spins along the field direction. This leads to the increase of the  $z$ -projection  $\langle S_z(\vec{R}) \rangle_0$  and to the increase of the barrier height  $W$  (9).

## 4 FM / SC heterostructures with quantum wells with spin-polarized localized electrons

Considering the IMR effect in  $\text{SiO}_2(\text{Co})/\text{GaAs}$  heterostructures, we can result in conclusion that for the efficient magnetoresistance and spin injection in FM / SC heterostructures it is need to fulfill the following requirements.

- (1) The SC contains a quantum well at the interface.
- (2) The quantum well must contain localized electron levels.
- (3) Localized levels must be exchange-split by the FM.
- (4) Giant magnetoresistance effect can be achieved on the base of the avalanche breakdown phenomena.

It is very important to extend the IMR effect observed in  $\text{SiO}_2(\text{Co})/\text{GaAs}$  heterostructures to heterostructures with other SCs and to reach high efficient spin-polarized electron injection. One of the promising semiconductor for spintronics with enhanced lifetime and transport length is silicon, Si [19, 47, 66]. Spin-orbit effects producing spin relaxation are much smaller in Si than in GaAs owing to the lower atomic mass and the inversion symmetry of the crystal structure maintaining spin-degenerate bands. Furthermore, the most abundant isotope  $^{28}\text{Si}$  has no nuclear spin, suppressing hyperfine interactions. These properties make relatively long spin lifetimes in Si.

The studied  $\text{SiO}_2(\text{Co})/\text{GaAs}$  heterostructures contain quantum wells formed by the  $\text{SiO}_2(\text{Co})$  film due to the difference of the chemical potentials between the  $\text{SiO}_2(\text{Co})$  and the GaAs. Using another methods to form quantum wells at interfaces in SCs (molecular beam epitaxy, MOCVD), we can obtain quantum wells with desired thickness, depth and number of localized electron levels. Localized levels can be splitted by the exchange interaction with a FM grown at the interface or by the interaction with a granular film containing FM nanoparticles. It is need to note that the latter technology method – sputtering of the granular film can solve the problem of the efficient spin injection difficulty due to the inherent conductivity mismatch between FM metals and SCs [67]. Variation of the FM nanoparticle concentration leads to considerable variation in the conductivity of the granular film and we can reach conductivity correspondence between the FM and the SC. In some cases, the combination FM metal layer with a granular film with FM nanoparticles can be used. In order to reach efficient spin polarization of injected electrons, we must increase energies  $\varepsilon_\lambda^{(\text{ex})}$  (6) of exchange-splitted levels and the height of the spin-dependent potential barrier  $W$  (9). The spin-polarized current is the sum of electrons surmounting the barrier and electrons tunneling from exchange-splitted states in the quantum well (Figure 13). Manipulation of the tunneling (increase of the tunneling transparency from the highest sublevel and suppression of the tunneling from other sublevels) can be realized by extending the region  $[\delta_1, \delta_2]$  and decreasing the potential energy in the region  $[\gamma_1, \gamma_2]$ .

Magnetic sensors and non-volatile magnetic memory storage cells can be constructed on the base of the spin-valve structure containing SC with two quantum wells and two FM layers, for example, Fe, Co, CoFe and NiFe alloys (figure 16). In order to overcome the conductivity mismatch, the combination FM metal layer with a granular film with FM nanoparticles sputtered on the SC interface can be used. In the spin-valve structure one of the FM layers is exchanged biased using an antiferromagnetic layer (for example, IrMn, Mn, Ru) and the second is free. The relative magnetizations of these FM layers can be modulated by manipulating an external field [46, 68, 69]. The FM layers have different magnetic coercivities to obtain parallel and anti-parallel alignment. If magnetizations of the layers are aligned parallel to one another, then spin-polarized electrons easy tunnel from sublevels of the first quantum well to sublevels of the second one. In the opposite case, if magnetizations of the layers are antialigned, then spin polarizations of these sublevels have anti-parallel alignment. This leads to sharp decreasing in the tunneling transparency. Thus, the manipulation of magnetic polarizations gives rise to an efficient spin-filter effect.

## 5 Conclusion

We have studied the electron spin transport in  $\text{SiO}_2(\text{Co})/\text{GaAs}$  and  $\text{SiO}_2(\text{Co})/\text{Si}$  heterostructures, where the  $\text{SiO}_2(\text{Co})$  structure is the granular  $\text{SiO}_2$  film with Co nanoparticles and have obtained the following results.

(1) In  $\text{SiO}_2(\text{Co})/\text{GaAs}$  heterostructures the giant injection magnetoresistance (IMR) effect is observed. The IMR effect has positive values and the temperature-peak type character. The temperature location of the effect depends on the Co concentration and can be shifted by the applied electrical field. For the  $\text{SiO}_2(\text{Co})/\text{GaAs}$  heterostructure with 71 at.% Co the IMR value reaches 1000 ( $10^5$  %) at room temperature, which is two-three orders higher than maximum values of GMR in metal magnetic multilayers and TMR in magnetic tunnel junctions. On the contrary, for  $\text{SiO}_2(\text{Co})/\text{Si}$  heterostructures magnetoresistance values are very small (4%) and for  $\text{SiO}_2(\text{Co})$  films the intrinsic magnetoresistance has an opposite value.

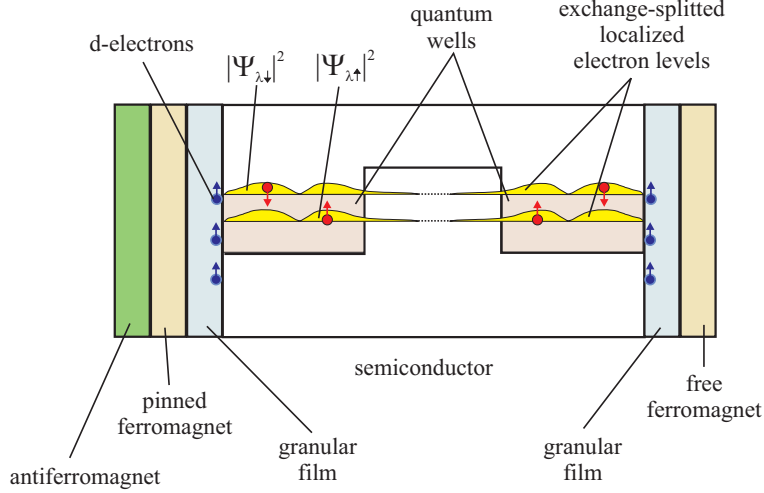


Figure 16: Schematic band diagram of the spin-valve structure on the base of the heterostructure with two granular films and two quantum wells.

(2) High values of the magnetoresistance effect in  $\text{SiO}_2(\text{Co})/\text{GaAs}$  heterostructures have been explained by magnetic-field-controlled process of impact ionization in the vicinity of the spin-dependent potential barrier formed in the accumulation electron layer in the semiconductor near the interface. Kinetic energy of electrons, which pass through the barrier and trigger the avalanche process, is reduced by the applied magnetic field. This electron energy suppression postpones the onset of the impact ionization to higher electric fields and results in the giant magnetoresistance. Although it is need a detailed theoretical model to understand the effect, the developed model can explain some features of experimental results. The spin-dependent potential barrier is due to the exchange interaction between electrons in the accumulation electron layer in the SC and  $d$ -electrons of Co. Existence of localized electron states in the accumulation layer results in the temperature-peak type character of the barrier and the IMR in the  $\text{SiO}_2(\text{Co})/\text{GaAs}$ . The temperature-peak type character distinguishes the spin-dependent potential barrier from the Schottky barrier. Maxima of peaks correspond to one exchange-split level in the accumulation layer. The temperature peak width is inversely proportional to the surface probability of the Co particle distribution at the interface. In contrast, for  $\text{SiO}_2(\text{Co})/\text{Si}$  heterostructures the accumulation layer has small thickness without any localized states, is tunnel transparent and does not influence on the injection current.

(3) FM/SC heterostructures with quantum wells with spin-polarized localized electrons in the SC at the interface are proposed as efficient room-temperature spin injectors and magnetic sensors.

## Acknowledgment

The authors gratefully acknowledge the assistance of Dr. V.M. Lebedev (PNPI, Gatchina, Leningrad region, Russia) for determination of the film composition, Dr. M.V. Baidakova (A.F. Ioffe Physico-Technical Institute, St. Petersburg, Russia) for the measurements by the small-angle X-ray scattering method, and S.Yu. Krasnoborod'ko (NT-MDT, Russia) for MFM images of the domain structure of samples. We would like to thank Prof. Yu.G. Kusrayev,

Dr. V.I. Kozub, and Dr. V.L. Korenev for useful discussions. This work was supported by the Russian Foundation for Basic Research.

## References

- [1] S.A. Wolf, D.D. Awschalom, R.A. Buhrman, J.M. Daughton, S. von Molnar, M.L. Roukes, A.Y. Chtchelkanova and D.M. Treger, *Science* **294**, 1488 (2001).
- [2] G. Schmidt, *J. Phys. D: Appl. Phys.* **38**, R107 (2005).
- [3] I. Žutić, J. Fabian, and S. Das Sarma, *Rev. Mod. Phys.* **76**, 323 (2004).
- [4] B.P. Zakharchenya and V.L. Korenev, *Physics-Uspekhi* **175**, 603 (2005).
- [5] R. Bertacco, M. Riva, M. Cantoni, F. Ciccacci, M. Portalupi, A. Brambilla, L. Duo, P. Vavassori, F. Gustavsson, J.-M. George, M. Marangolo, M. Eddrief, and V.H. Etgens, *Phys. Rev. B* **69**, 054421 (2004).
- [6] G. Schmidt, G. Richter, P. Grabs, C. Gould, D. Ferrand, and L.W. Molenkamp, *Phys. Rev. Letters* **87**, 227203 (2001).
- [7] Y. Ohno, D.K. Yong, B. Beschoten, F. Matsukura, F. Ohno, and D.D. Awschalom, *Nature* **402**, 790 (1999).
- [8] B.T. Jonker, Y.D. Park, B.R. Bennett, H.D. Cheong, G. Kioseoglou, and A. Petrou, *Phys. Rev. B* **62**, 8180 (2000).
- [9] A. Hirohata, Y.B. Xu, C.M. Guertler, and J.A.C. Bland, *J. Appl. Phys.* **87**, 4670 (2000).
- [10] A. Hirohata, Y.B. Xu, C.M. Guertler, J.A.C. Bland, and S.N. Holmes, *Phys. Rev. B* **63**, 104425 (2001).
- [11] A.F. Isakovic, D.M. Carr, J. Strand, B.D. Schultz, C.J. Palmstrøm, and P.A. Crowell, *Phys. Rev. B* **64**, 161304 (2001).
- [12] Z.H. Xiong, D. Wu, Z.V. Vardeny, and J. Shi, *Nature* **427**, 821 (2004).
- [13] A.T. Hanbicki, B.T. Jonker, G. Istkos, G. Kioseoglou, and A. Petrou, *Appl. Phys. Lett.* **80**, 1240 (2002).
- [14] H.J. Zhu, M. Ramsteiner, H. Kostial, M. Wassermeier, H.-P. Schönherr, and K.H. Ploog, *Phys. Rev. Letters* **87**, 016601 (2001).
- [15] P.R. Hammar, B.R. Bennett, M.J. Yang, and M. Johnson, *Phys. Rev. Letters* **83**, 203 (1999).
- [16] P.R. Hammar and M. Johnson, *Appl. Phys. Letters* **79**, 2591 (2001).
- [17] X. Jiang, R. Wang, R.M. Shelby, R.M. Macfarlane, S.R. Bank, J.S. Harris, and S.S.P. Parkin, *Phys. Rev. Letters* **94**, 056601 (2005).

- [18] R. Mattana, J.-M. George, H. Jaffres, F. Nguyen Van Dau, and A. Fert, *Phys. Rev. Letters* **90**, 166601 (2003).
- [19] B.T. Jonker, G. Kioseoglou, A.T. Hanbicki, C.H. Li, and P.E. Thompson, *Nature Physics* **3**, 542 (2007).
- [20] M.N. Baibich, J.M. Broto, A. Fert, F. Nguyen Van Dau, F. Petroff, P. Eitenne, G. Creuzet, A. Friederich, and J. Chazelas, *Phys. Rev. Lett.* **61**, 2472 (1988).
- [21] G. Binasch, P. Grunberg, F. Saurenbach, and W. Zinn, *Phys. Rev. B* **39**, 4828 (1988).
- [22] J. Bass and W.P. Pratt, Jr., *J. Magn. Magn. Mater.* **200**, 274 (1999).
- [23] M.A.M. Gijs and G.E.W. Bauer, *Adv. Phys.* **46**, 285 (1997).
- [24] J.S. Moodera, L.R. Kinder, T.M. Wong, and R. Meservey, *Phys. Rev. Lett.* **74**, 3273 (1995).
- [25] J.S. Moodera and G. Mathon, *J. Magn. Magn. Mater.* **200**, 248 (1999).
- [26] Xiu-Feng Han, M. Oogane, H. Kubota, Y. Ando, and T. Miyazaki, *Appl. Phys. Lett.* **77**, 283 (2000).
- [27] E.Y. Tsymbal, O.N. Mryasov, and P.R. LeClair, *J. Phys.: Condens. Matter* **15**, R109 (2003).
- [28] J.M. De Teresa, A. Barthelemy, A. Fert, J.P. Contour, F. Montaigne, and P. Seneor, *Science* **286**, 507 (1999).
- [29] X. Jiang, R. Wang, R. Shelby, R.M. Macfarlane, S.R. Bank, J.S. Harris, and S.S.P. Parkin *Phys. Rev. Lett.* **94**, 056601 (2005).
- [30] S.S.P. Parkin, C. Kaiser, A. Panchula, P.M. Rice, B. Hughes, M. Samant, and S.-H. Yang, *Nature Materials* **3**, 862 (2004).
- [31] S. Yuasa, T. Nagahama, A. Fukushima, Y. Suzuki, and K. Ando, *Nature Materials* **3**, 868 (2004).
- [32] S. Yuasa, A. Fukushima, H. Kubota, Y. Suzuki, and K. Ando, *Applied Physics Letters* **89**, 042505 (2006).
- [33] C. Tiusan, F. Greullet, M. Hehn, F. Montaigne, S. Andrieu, and A. Schuhl, *J. Phys.: Condens. Matter* **19**, 165201 (2007).
- [34] Y.M. Lee, J. Hayakawa, S. Ikeda, F. Matsukura, and H. Ohno, *Applied Physics Letters* **90**, 212507 (2007).
- [35] V.A. Samuilov, V.K. Ksenevich, G. Remenyi, G. Kiss, and B. Pödör, *Semicond. Sci. Technol.* **14**, 1084 (1999).
- [36] H. Akinaga, M. Mizuguchi, K. Ono, and M. Oshima, *Applied Physics Letters* **76**, 357 (2000).

- [37] Z.G. Sun, M. Mizuguchi, T. Manago, and H. Akinaga, *Applied Physics Letters* **85**, 5643 (2004).
- [38] L.V. Lutsev, A.I. Stognij, and N.N. Novitskii, *JETP Letters* **81**, 514 (2005).
- [39] L.V. Lutsev, A.I. Stognij, N.N. Novitskii, and A.A. Stashkevich, *J. Magn. Magn. Mater.* **300**, e12 (2006).
- [40] L.V. Lutsev, *J. Phys.: Condens. Matter* **18**, 5881 (2006).
- [41] M. Yokoyama, T. Ogawa, A.M. Nazmul, and M. Tanaka, *J. Appl. Phys.* **99**, 08D502 (2006).
- [42] J.J.H.M. Schoonus, F.L. Bloom, W. Wagemans, H.J.M. Swagten, and B. Koopmans *Phys. Rev. Lett.* **100**, 127202 (2008).
- [43] J.J.H.M. Schoonus, J.T. Kohlhepp, H.J.M. Swagten, and B. Koopmans *J. Appl. Phys.* **103**, 07F309 (2008).
- [44] J. Nordling, R.L. Millen, H.A. Bullen, M.D. Porter, M. Tondra, and M.C. Granger, *Anal. Chem.* **80**, 7930 (2008).
- [45] R.L. Millen, J. Nordling, H.A. Bullen, M.D. Porter, M. Tondra, and M.C. Granger, *Anal. Chem.* **80**, 7940 (2008).
- [46] I. Appelbaum, K.J. Russel, D.J. Monsma, V. Narayanamurti, C.M. Marcus, M.P. Hanson, and A.C. Gossard, *Applied Physics Letters* **83**, 4571 (2003).
- [47] I. Appelbaum and D.J. Monsma, *Applied Physics Letters* **90**, 262501 (2007).
- [48] K.J. Russel, I. Appelbaum, Wei Yi, D.J. Monsma, F. Capasso, C.M. Marcus, V. Narayanamurti, M.P. Hanson, and A.C. Gossard, *Applied Physics Letters* **85**, 4502 (2004).
- [49] A.I. Stognij, N.N. Novitskii, and O.M. Stukalov, *Tech. Phys. Lett.* **28**, 17 (2002).
- [50] A.I. Stognij, N.N. Novitskii, and O.M. Stukalov, *Tech. Phys. Lett.* **29**, 43 (2003).
- [51] T.K. Zvonareva, V.M. Lebedev, T.A. Polanskaya, L.V. Sharonova, and V.I. Ivanov-Omskii, *Semiconductors* **34**, 1094 (2000).
- [52] S. Barzilai, Y. Goldstein, I. Balberg, and J.S. Helman, *Phys. Rev. B* **23**, 1809 (1981).
- [53] K. Yakushiji, S. Mitani, K. Takanashi, J.-G. Ha, and H. Fujimori, *J. Magn. Magn. Mater.* **212**, 75 (2000).
- [54] S. Sankar, D. Dender, J.A. Borchers, D.J. Smith, R.W. Erwin, S.R. Kline, and A.E. Berkowitz, *J. Magn. Magn. Mater.* **221**, 1 (2000).
- [55] Yu.A. Izyumov, F.A. Kassan-ogly, and Yu.N. Skryabin, *Field Methods in the Theory of Ferromagnetism* (Nauka, Moscow, 1974).

- [56] A.A. Abrikosov , L.P. Gor'kov, and I.E. Dzyaloshinski, *Methods of Quantum Field Theory in Statistical Physics* (Dover, New York, 1975).
- [57] M.A. Ruderman and C. Kittel, Phys. Rev. **96**, 99 (1954).
- [58] T. Kasuya, Prog. Theor. Phys. **16**, 45 (1956).
- [59] K. Yosida, Phys. Rev. **106**, 893 (1957).
- [60] W.A. Harrison, *Electronic Structure and the Properties of Solids. The Physics of the Chemical Bond* (W.H. Freeman and Company, San Francisco, 1980).
- [61] J.J. Mareš, J. Křištofik, P. Hubik, K. Jurek, S. Pospíšil, and J. Kubašta, J. Appl. Phys. **82**, 3358 (1997).
- [62] L.D. Landau and E.M. Lifshitz, *Quantum Mechanics. Non-relativistic Theory* (Pergamon, New York, 1977).
- [63] M.P. Delmo, S. Yamamoto, S. Kasai, T. Ono, and K. Kobayashi, Nature **457**, 1112 (2009).
- [64] V.S. Fomenko and I.A. Podchernyaeva, *Emission and Adsorption Properties of Substances and Materials* (Nauka, Moscow, 1975).
- [65] *Handbook of Physical Quantities*, Ed. by I.S. Grigoriev and E.Z. Meilikhov (CRC Press, Boca Raton, 1997).
- [66] I. Appelbaum, B. Huang, and D.J. Monsma, Nature **447**, 295 (2007).
- [67] G. Schmidt, D. Ferrand, L.W. Molenkamp, A.T. Filip, and B.J. van Wees, Phys. Rev. B **62**, R4790 (2000).
- [68] I. Appelbaum, D.J. Monsma, K.J. Russel, V. Narayanamurti, and C.M. Marcus, Applied Physics Letters **83**, 3737 (2003).
- [69] B. Dieny, V.S. Speriosu, B.A. Gurney, S.S.P. Parkin, D.R. Wilhoit, K.P. Roche, S. Metin, D.T. Peterson, and S. Nadimi, J. Magn. Magn. Mater. **93**, 101 (1991).